Redox Biology 59 (2023) 102564

Contents lists available at ScienceDirect

Redox Biology

journal homepage: www.elsevier.com/locate/redox

Increased ATF2 expression predicts poor prognosis and inhibits sorafenib-induced ferroptosis in gastric cancer

Xin Xu [a,b], Yaxian Li [a,b], Youliang Wu [a], Mingliang Wang [a], Yida Lu [a,b], Ziqing Fang [a,b], Huizhen Wang [a], Yongxiang Li [a,*]

[a] Department of General Surgery, The First Affiliated Hospital of Anhui Medical University, Hefei, 230022, China
[b] Anhui Medical University, Hefei, 230022, China

ARTICLE INFO

Keywords:
Gastric cancer
Sorafenib
ATF2
HSPH1
Ferroptosis

ABSTRACT

Sorafenib, a tyrosine kinase inhibitor, has an important antitumor effect as a ferroptosis inducer in multiple cancers, including gastric cancer (GC). However, the status of sorafenib as a ferroptosis inducer has recently been questioned. There is very limited information about the relationship between ferroptosis and ATF2, and the role of ATF2 in sorafenib-induced ferroptosis has not been studied. In this study, we investigated the role and underlying molecular mechanisms of ATF2 in sorafenib-induced ferroptosis in GC. We found that ATF2 was significantly upregulated in GC tissues and predicted a poor clinical prognosis. Silencing ATF2 significantly inhibited the malignant phenotype of GC cells. In addition, we observed that ATF2 was activated during sorafenib-induced ferroptosis in GC cells. ATF2 knockdown promoted sorafenib-induced ferroptosis, while ATF2 overexpression showed the opposite results in GC cells. Using ChIP-Seq and RNA-Seq, we identified HSPH1 as a target of ATF2 and further validated it by ChIP–qPCR analysis. HSPH1 can interact with SLC7A11 (cystine/glutamate transporter) and increase its protein stability. Importantly, knockdown of HSPH1 partly reversed the effects caused by ATF2 overexpression on sorafenib-induced ferroptosis in GC cells. In addition, the results from the tumor xenograft model showed that ATF2 knockdown can effectively enhance sorafenib sensitivity in vivo. Collectively, our study reveals a novel mechanism by which sorafenib induces ferroptosis in GC.

1. Introduction

Gastric cancer (GC) is one of the most commonly diagnosed tumors and ranks as the fourth leading cause of cancer-related deaths worldwide [1]. Patients in China account for approximately half of all cases worldwide, and most patients are already at an advanced stage at the time of initial diagnosis [2]. The prognosis of GC patients remains poor despite great advances in treatment over the past decades, including surgery, chemotherapy, radiation, immunotherapy and a combined approach [3]. Therefore, it is urgent to identify effective therapeutic strategies and targets for the treatment of GC patients.

Ferroptosis, a novel form of programmed cell death, is characterized by lipid peroxidation products accumulating in a cellular-iron dependent manner [4]. Inhibition of cystine/glutamate transporter (SCL7A11 or xCT, also known as system Xc-) and glutathione peroxidase 4 (GPX4) are the most common methods to induce ferroptosis [5]. To date, ferroptosis has been shown to be effective in killing various cancer cells, including GC. Sorafenib restricts cystine input by inhibiting system Xc-, causing endoplasmic reticulum stress, glutathione depletion and iron-dependent accumulation of lipid reactive oxygen species (ROS) and finally inducing ferroptosis [6–8]. Although sorafenib has not been used clinically for treatment of GC, its encouraging anticancer effect in GC has been reported by several studies [9–11]. Notably, considering the adverse side effects of sorafenib, combination therapy may have better clinical prospects to achieve a low dose with high efficacy. In addition, a recent study pointed out that sorafenib does not trigger ferroptosis in all tumor cell lines and questioned its adequacy as a ferroptosis inducer [12]. Thus, whether sorafenib can actually induce ferroptosis in GC cells and the underlying molecular mechanism remain largely unknown.

Activation transcription factor 2 (ATF2), a member of the ATF/CREB family of transcription factors (TFs), has been implicated in a broad spectrum of cancer-related biological functions, such as cell proliferation, apoptosis and DNA repair [13,14]. Growing evidence indicates that ATF2 acts as an oncogene or a tumor suppressor in different cancer types

* Corresponding author. Department of General Surgery, The First Affiliated Hospital of Anhui Medical University, 218 JiXi Avenue, Hefei, 230022, Anhui, China.
E-mail address: liyongxiang@ahmu.edu.cn (Y. Li).

https://doi.org/10.1016/j.redox.2022.102564
Received 31 October 2022; Received in revised form 21 November 2022; Accepted 28 November 2022
Available online 2 December 2022

Table 1
Correlation of ATF2 expression with clinicopathologic parameters in GC patients.

Parameters	Cases	ATF2 expression		χ^2	*P*-value
		High	Low		
Gender				1.383	0.240
Male	71	41	30		
Female	36	25	11		
Age (years)				0.382	0.537
<61	43	25	18		
≥61	64	41	23		
Tumor location				0.570	0.450
Upper	36	24	12		
Middle + lower	71	42	29		
Tumor size (cm)				0.915	0.339
<6	48	32	16		
≥6	59	34	25		
Depth of invasion				1.669	0.196
T1 + T2	29	15	14		
T3 + T4	78	51	27		
Lymph node metastasis				8.969	0.003[a]
Absent	23	8	15		
Present	84	58	26		
Differentiation				1.811	0.178
Well + moderate	41	22	19		
Poor + undifferentiated	66	44	22		
TNM stage				4.509	0.034[a]
I + II	34	16	18		
III + IV	73	50	23		

[a] Statistically significant ($P < 0.05$).

depending on its expression level and subcellular localization [15]. Generally, in response to many forms of cellular stress, especially oxidative stress, ATF2 is phosphorylated by multiple upstream kinases, translocates to the nucleus and increases transcriptional activity [16]. Although the oncogenic role of ATF2 in GC has been reported in several studies [17–19], there is still a lack of experimental evidence in vitro and in vivo, especially its relationship with clinicopathological parameters and prognosis.

In this study, we confirmed that sorafenib can induce ferroptosis in GC cells, and observed an accompanying increase in the phosphorylation level and transcriptional activity of ATF2. We found increased ATF2 expression in GC and that it is associated with a malignant phenotype and poor prognosis. Inhibition of ATF2 expression in vitro and in vivo increased sorafenib-induced ferroptosis in GC. Mechanistically, ATF2 protects GC cells from sorafenib-mediated ferroptosis by inhibiting SLC7A11 protein degradation through the promotion of the expression of heat shock protein-110 (HSPH1, also called HSP105 or HSP110). Here, we demonstrate that promoting sorafenib-induced ferroptosis may be a promising new strategy for GC treatment.

2. Materials and methods

2.1. Patient samples and follow-up

In the present study, a total of 107 formalin-fixed paraffin-embedded GC tissues and 22 randomly selected corresponding adjacent normal tissues following radical gastrectomy without preoperative chemotherapy or radiotherapy were obtained from the First Affiliated Hospital of Anhui Medical University between October 2012 and December 2013 for tissue microarray (TMA) construction. The follow-up time ranged from 8 months to 71 months. The clinical and pathological data are summarized in Table 1, and the GC patients were staged according to the 8th edition AJCC staging system. Additionally, 12 fresh primary cancer and paired adjacent normal tissue specimens were also collected. The Ethics Committee of Anhui Medical University approved the study, and written informed consent was obtained from all the patients enrolled in this study.

2.2. Cell culture, lentiviral infection and siRNA transfection

The normal gastric epithelial cell line GES-1 and the GC cell lines SGC7901, HGC27, AGS, MGC803 and MKN45 were obtained from GeneChem (Shanghai, China). The cells were cultured in RPMI 1640 medium (Corning, NY, USA) supplemented with 10% fetal bovine serum (FBS, Clark Bioscience, Richmond, VA, USA) and 1% penicillin–streptomycin (HyClone, Logan, UT, USA) in a humidified incubator at 37 °C containing 5% CO_2.

The ATF2-overexpressing lentiviral GV341 vector (Ubi-MCS-3FLAG-SV40-puromycin), ATF2 small hairpin RNA (shRNA) lentiviral GV112 vector (hU6-MCS-CMV-puromycin) and control lentiviral vector were constructed by GeneChem (Shanghai, China). Small interfering RNA (siRNA) against HSPH1 and control siRNA were purchased from Hippo Biotechnology (Huzhou, China). To generate stable ATF2 knockdown and overexpression cell lines, the cells were infected with lentivirus at an MOI of 10 and then selected with 2 μg/ml puromycin for 2 weeks. The established stable cell lines were maintained in 1 μg/ml puromycin for further experiments. For HSPH1 siRNA transfection, the cells were seeded at 50% confluency and transfected with siRNA duplexes at a final concentration of 30 nM for 48 h using LipoJet reagent (SignaGen, Rockville, MD, USA) according to the manufacturer's protocol. The shRNA and siRNA sequences are listed in Table S1.

2.3. Western blot analysis

Total proteins were extracted using mammalian protein extraction reagent (M-PER) (#78501, Thermo Scientific, USA) supplemented with protease and phosphatase inhibitor cocktails. Protein concentrations were determined using a BCA protein assay kit (A045-4, Jiancheng Bioengineering Institute, Nanjing, China). Equal amounts of protein samples were separated by SDS-polyacrylamide gel electrophoresis and then transferred onto PVDF membranes (Millipore, MA, USA). After blocking in 5% skim milk in TBST for 1 h at room temperature, the membranes were incubated with primary antibodies against ATF2 (1:1000, ab32160, Abcam, Cambridge, UK), p-ATF2 (1:1,000, sc-8398, Santa Cruz Biotechnology, TX, USA), SLC7A11 (1:1000, ab175186, Abcam, Cambridge, UK), HSPH1 (1:1000, ab109624, Abcam, Cambridge, UK), and GAPDH (1:2500, #5174, Cell Signaling Technology, MA, USA) overnight at 4 °C. Following incubation with the secondary antibody for 1 h at room temperature, the protein bands were visualized using enhanced chemiluminescence (Bridgen, Beijing, China) and imaged using a Tanon-5200 chemiluminescence detection system (Tanon Science, Shanghai, China).

2.4. Quantitative real-time polymerase chain reaction (qRT–PCR)

Total RNA was extracted from cells using TRIzol (Invitrogen, CA, USA), and then cDNA was synthesized with Hifair® III 1st Strand cDNA Synthesis SuperMix for qPCR (11141ES60, Yeasen Biotechnology, Shanghai, China). Subsequently, qPCR was performed using Hieff® qPCR SYBR Green Master Mix (11202ES03, Yeasen Biotechnology, Shanghai, China) on the Agilent Mx3000P qPCR Platform (Agilent, CA, USA). Relative gene expression was calculated using the $2^{-\Delta\Delta Ct}$ method, and GAPDH served as an internal control. All primers were synthesized by General Biosystems (Anhui, China) and are shown in Table S2.

2.5. Immunohistochemical staining

ATF2 protein expression was evaluated by immunohistochemistry (IHC) in a TMA as described previously [20]. The TMA was incubated with anti-ATF2 (1:500 dilution) and then scored independently for staining area (0, no staining; 1, 0–25%; 2, 26%–50%; 3, 51%–75%; 4, 76%–100%) and staining intensity (0, negative; 1, weak; 2, moderate; 3, strong) by two clinical pathologists. The final score was the product of the staining area and the staining intensity. High expression was defined

as a final score of ≥5, and low expression was defined as a final score of 0–4.

2.6. Cell growth curve

For cell growth curve analysis, GC cells were plated onto 96-well plates at a density of 5×10^3 cells per well. At the indicated times, 10 μL of Cell Counting Kit-8 (CCK-8; 40203ES76, Yeasen Biotechnology, Shanghai, China) solution was added to each well, followed by incubation at 37 °C for 1 h. The relative optical density (OD) was measured at 450 nm using a microplate reader (Biotek, USA).

2.7. Half-maximal inhibitory concentration (IC50) assay

GC cells were seeded at 1×10^4 cells per well in 96-well plates and treated with a range of concentrations of sorafenib (0–80 μM) for 24 h. Ten microliters of CCK-8 solution was added to each well and incubated for 1 h at 37 °C. The absorbance was measured at 450 nm using a microplate reader (Biotek, USA), and IC50 values were calculated using GraphPad Prism software 6.0 (GraphPad Software, Inc., San Diego, CA, USA).

2.8. Transwell migration and invasion assays

Cell migration and invasion assays were performed using 24-well Transwell chambers with a pore size of 8 μm (Corning, USA). Briefly, 8×10^4 GC cells were seeded in the upper chamber with Matrigel (BD Biosciences, USA) for the invasion assay or without Matrigel for the migration assay. Then, 650 μl of culture medium containing 20% FBS was added to the lower chamber. After incubation for 24 h, the GC cells were fixed with 4% paraformaldehyde and stained with 0.1% crystal violet. Finally, the nonmigrating or noninvading cells were carefully removed with a wet cotton swab and then photographed under a Leica microscope (DMI1; Wetzlar, Germany).

2.9. Calcein-AM/PI staining

Live/dead cell staining was performed using a calcein-AM/PI Double Staining Kit (C2015S, Beyotime, Shanghai, China) according to the protocol. After different treatments, the GC cells were washed with PBS and stained by a mixture of calcein-AM and PI solution for 30 min at 37 °C in the dark. Fluorescence signals were analyzed with a fluorescence microscope. Live cells appeared green due to calcein-AM staining, while dead cells appeared red after PI staining.

2.10. Intracellular reactive oxygen species (ROS) and lipid peroxidation detection

Intracellular ROS levels were determined using DCFH–DA (D6883, Sigma, MO, USA). In brief, cultured GC cells in 6-well plates were incubated with 5 μM DCFH-DA in serum-free medium at 37 °C for 30 min in the dark. After washing three times with PBS, the cells were resuspended in 500 μL of PBS and then analyzed by flow cytometry (Beckman Coulter, CA, USA). For lipid peroxidation detection, GC cells were loaded with 1 ml of fresh medium containing 10 μM C11 BODIPY 581/591 (GC40165, GlpBio, CA, USA) for 30 min at 37 °C. Following two washes with PBS, the cells were resuspended in 500 μL of PBS containing 5% FBS for flow cytometry analysis.

2.11. MDA and glutathione (GSH) detection

MDA is a final product of lipid peroxidation, which shows a positive correlation with ferroptosis [21]. The MDA concentration in GC cells was measured by the thiobarbituric acid method using a cell MDA assay kit (A003-4, Jiancheng Bioengineering Institute, Nanjing, China). MDA was calculated based on cellular protein concentration and expressed as nmol of MDA per milligram of protein (nmol/mgprot).

The lethal metabolic imbalance resulted from GSH depletion is a major feature of ferroptosis [4]. For GSH detection, a Micro Reduced Glutathione Assay Kit (BC1175, Solarbio, Beijing, China) was used according to the manufacturer's instructions. The concentration of cellular GSH was determined from a GSH standard curve and normalized to the cell number.

2.12. Mitochondrial membrane potential (MMP) measurement

The change in MMP was assessed using a JC-1 MMP Assay Kit (40706ES60, Yeasen Biotechnology, Shanghai, China). Briefly, after incubating with JC-1 staining work solution for 20 min at 37 °C, the GC cells were washed twice with JC-1 staining buffer and imaged using a fluorescence microscope. The red fluorescent aggregate indicates a healthy mitochondrion with normal membrane potential, whereas the green fluorescent monomer indicates loss of MMP.

2.13. Transmission electron microscopy (TEM)

After treatment with sorafenib (HY-10201, MedChemExpress, NJ, USA), ferrostatin-1 (Fer-1, HY-100579, MedChemExpress, NJ, USA) or DMSO for 24 h, the cells were fixed in 4% paraformaldehyde (P0099, Beyotime, Shanghai, China) for 2 min. Following cell harvest by centrifugation, 2.5% glutaraldehyde (P1126; Solarbio, Beijing, China) was carefully added to the cell pellet along the tube wall. Finally, ultrathin sections were cut, and the morphological changes of mitochondria were observed under TEM (TECNA I20; Philips, Eindhoven, Netherlands).

2.14. RNA sequencing (RNA-seq) analysis

RNA-seq was carried out by Seqhealth Technology Co., Ltd. (Wuhan, China). Total RNA was extracted from MGC803 cells with lentivirus-mediated knockdown of ATF2 (sh-ATF2) or the negative control (sh-Ctrl). After RNA quality evaluation and library preparation, the library products were further sequenced with the Illumina NovaSeq 6000 sequencing platform. Differentially expressed genes (DEGs) were screened using thresholds of $|\log2 \text{(fold change)}| > 1$ and p-value <0.05.

2.15. Chromatin immunoprecipitation-sequencing (ChIP-seq) and ChIP–qPCR

The ChIP assay and high-throughput sequencing were conducted by Seqhealth Technology Co., Ltd. (Wuhan, China). Briefly, approximately 2×10^7 AGS cells stably overexpressing ATF2 were fixed in 1% formaldehyde for 10 min at room temperature, after which 125 mM glycine was added and left for 5 min to terminate the crosslinking reaction. After ChIP lysis buffer (5 mM PIPES, pH 8.0, 85 mM KCl, 0.5% NP-40, protease inhibitors) treatment, the nuclear pellet was collected by centrifugation at 2000×g for 5 min at 4 °C. The chromatin was sonicated to an average DNA fragment length of 200–500 bp and then incubated with ChIP-grade antibody against ATF2 (ab32160, Abcam, Cambridge, UK) at 4 °C overnight for chromatin immunoprecipitation. After DNA extraction with the phenol–chloroform method, the purified products were sequenced on a NovaSeq 6000 sequencer (Illumina) with a PE150 model. The raw sequencing data were evaluated using FastQC and filtered by Trimmomatic. MACS2 (narrow peak mode) was used for peak calling with a p-value threshold of 0.01. In addition, de novo motif analysis of the ATF2 binding site was performed with HOMER software.

For ChIP–qPCR, immunoprecipitation was performed at 4 °C overnight with anti-ATF2 or normal rabbit IgG antibody. Then, qRT–PCR was utilized to quantify the immunoprecipitated DNA, and the data were normalized to the input. The primers used for ChIP–qPCR are listed in Table S2.

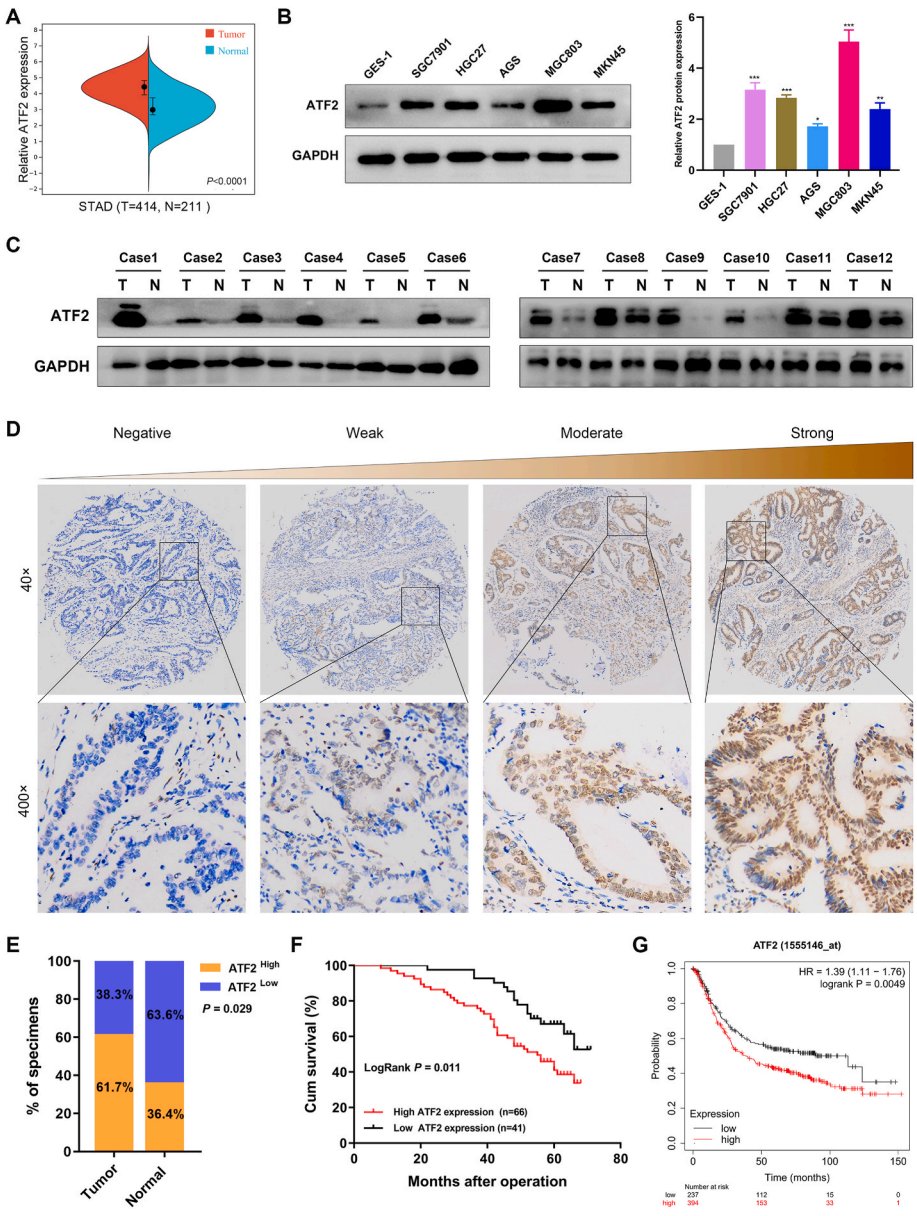

Fig. 1. ATF2 is upregulated in GC and predicts a poor prognosis. **(A)** The expression of ATF2 was determined based on the TCGA databases. **(B)** Western blot was used to detect the protein level of ATF2 in the GES-1 and GC cell lines. **(C)** ATF2 expression was analyzed by Western blot in GC and adjacent normal tissues. **(D)** Representative ATF2 IHC staining images in GC tissue microarray. **(E)** The statistical analysis of ATF2 expression in GC and adjacent normal tissues. The final score was the product of the staining area and the staining intensity. High expression was defined as a final score of ≥5, and low expression was defined as a final score of 0–4. **(F)** Kaplan–Meier survival curve of GC patients with low and high ATF2 expression in our study. **(G)** Kaplan-Meier survival curve of ATF2 expression was obtained from the KM plotter database. Data are shown as the mean ± SD (n = 3). $^{*}P < 0.05$, $^{**}P < 0.01$, $^{***}P < 0.001$.

2.16. Coimmunoprecipitation (co-IP)

GC cells were lysed in ice-cold M-PER buffer supplemented with protease and phosphatase inhibitor cocktails. After preclearing with 20 μl of protein A/G plus-agarose (sc-2003; Santa Cruz Biotechnology, USA) at 4 °C for 30 min, the cell lysates were incubated with anti-HSPH1, anti-SLC7A11, or IgG at 4 °C overnight on a gyratory shaker. Following incubation with 20 μl of protein A/G plus-agarose at 4 °C for 6 h, immunoprecipitated beads were washed with ice-cold lysis buffer three times and boiled in 50 μL of 1 × SDS sample buffer for 8 min at 95 °C. Then, the immunoprecipitated protein complexes were analyzed by western blotting. To avoid the influence of the heavy chain, a specific secondary antibody against the mouse anti-rabbit IgG light chain (A25022, Abbkine Scientific, Wuhan, China) was used.

2.17. Protein stability assay

To assess SLC7A11 protein stability, a cycloheximide (CHX) chase assay was performed. Cells were treated with 20 μg/ml CHX (S7418, Selleck Chemicals, TX, USA) for the indicated time periods (0, 2, 4, 6, and 8 h). Cell lysates were collected and analyzed by western blotting with GAPDH as a loading control.

2.18. Xenograft mouse model

Animal studies were approved by the Ethics Committee for Animal Studies of Anhui Medical University. Four-week-old female BALB/c nude mice were purchased from SLAC Laboratory Animal Co., Ltd. (Shanghai, China) and maintained under special pathogen-free (SPF) conditions. For subsequent studies, the nude mice were randomly divided into four groups as follows: sh-Ctrl, sh-ATF2, sh-Ctrl + sorafenib and sh-ATF2 + sorafenib. Approximately 5×10^6 ATF2 knockdown or control MGC803 cells were subcutaneously injected into the axilla of nude mice. Beginning on Day 8, mice in the sorafenib treatment group received 10 mg/kg sorafenib by intraperitoneal injection every 2 days for 3 weeks. Tumor length (L) and width (W) were measured every 3 days, and tumor volume (V) was calculated as follows: $(3.14 \times L \times W^2)/6$. Finally, all the mice were sacrificed and dissected immediately to measure the tumor weights. Tumors were fixed in 4% paraformaldehyde and stained with ATF2 antibody (1:500) or 4-hydroxynonenal (4-HNE)

Table 2
Univariate and multivariate analysis of clinicopathological variables and ATF2 expression associated with overall survival.

Parameters	Univariate analysis		Multivariate analysis	
	HR (95% CI)	P-value	HR (95% CI)	P-value
Gender (male vs female)	0.910 (0.511–1.622)	0.750		
Age (years) (<61 vs ≥ 61)	1.272 (0.732–2.212)	0.393		
Tumor location (upper vs middle + lower)	1.153 (0.643–2.068)	0.634		
Tumor size (cm) (<6 vs ≥ 6)	0.824 (0.482–1.408)	0.479		
Depth of invasion (T1 + T2 vs T3 + T4)	1.578 (0.827–3.008)	0.166		
Lymph node metastasis (absent vs present)	3.713 (1.474–9.353)	0.005[a]	3.254 (1.095–9.667)	0.034[a]
Differentiation (well + moderate vs poor + undifferentiated)	1.648 (0.918–2.957)	0.094		
TNM stage (I + II vs III + IV)	1.967 (1.034–3.739)	0.039[a]	1.026 (0.484–2.173)	0.946
ATF2 expression (low vs high)	2.122 (1.169–3.853)	0.013[a]	1.850 (1.013–3.379)	0.045[a]

[a] Statistically significant ($P < 0.05$).

antibody (1:100, ab48506, Abcam, Cambridge, UK) for IHC analysis.

2.19. Bioinformatic analysis

We downloaded the gastric cancer mRNA data from The Cancer Genome Atlas (TCGA) (https://tcga-data.nci.nih.gov/tcga/) and performed bioinformatic analysis using Sangerbox (http://www.sangerbox.com/tool). The survival curve of GC patients with high and low ATF2 expression was generated using Kaplan–Meier Plotter (www.kmplot.com). The GeneMANIA (http://genemania.org/) online database was used to predict potential interactions between ATF2 target genes and SLC7A11.

2.20. Statistical analysis

The statistical analysis was performed using SPSS 22.0 (SPSS Inc., USA) and GraphPad Prism 7.0 (GraphPad Software Inc., USA). All data are shown as the mean ± standard deviation (SD) and were compared using a Student's t-test or one-way ANOVA. The relationship between ATF2 expression and pathological variables was analyzed using Pearson's chi-squared test. Survival analysis was performed by the Cox proportional hazards regression model and Kaplan–Meier method with the log-rank test. $P < 0.05$ was considered significant ($^*P < 0.05$; $^{**}P < 0.01$; $^{***}P < 0.001$).

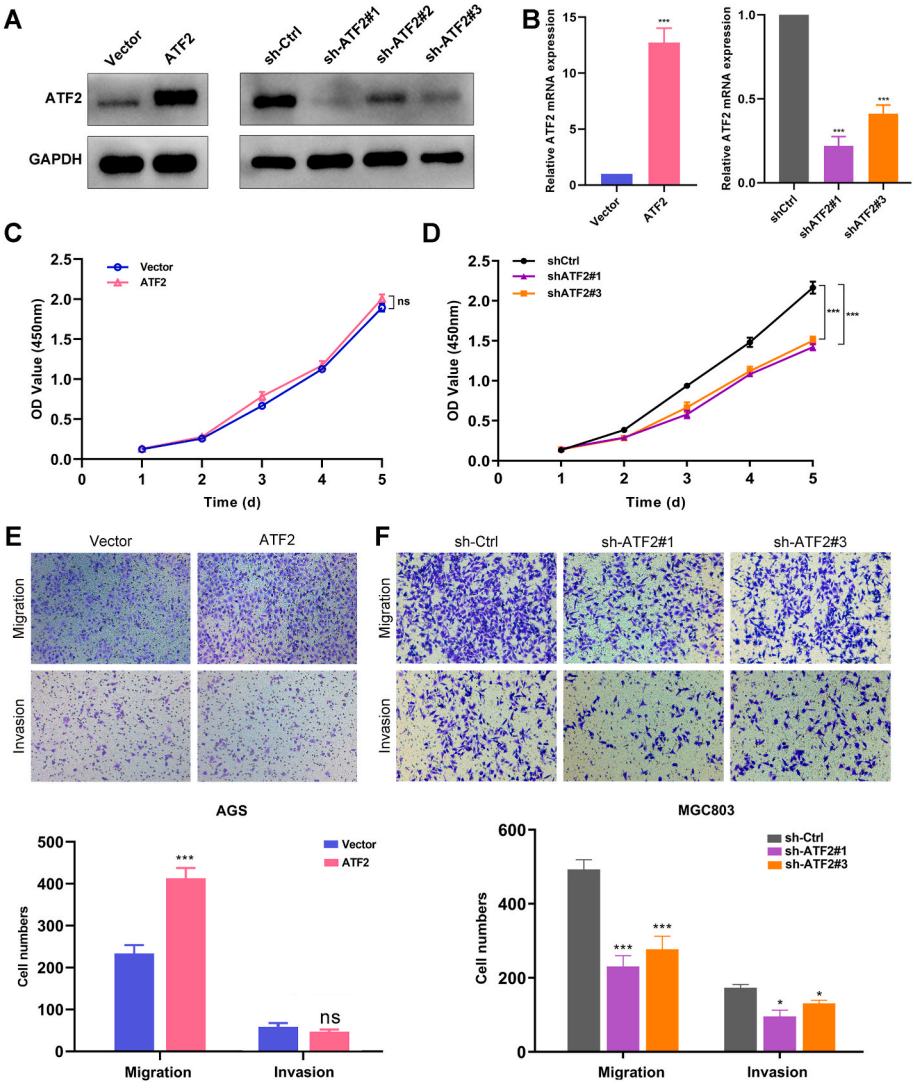

Fig. 2. ATF2 knockdown inhibits GC cell malignant phenotypes. **(A-B)** The overexpression and knockdown efficiency of ATF2 were confirmed by Western blot analysis and qRT-PCR. **(C–D)** CCK-8 assays were used to evaluate the effect of ATF2 overexpression or knockdown on GC cell proliferation. **(E–F)** The migratory and invasive ability of the indicated stable transfection GC cells were detected using Transwell assays. Data are shown as the mean ± SD (n = 3). $^*P < 0.05$, $^{**}P < 0.01$, $^{***}P < 0.001$.

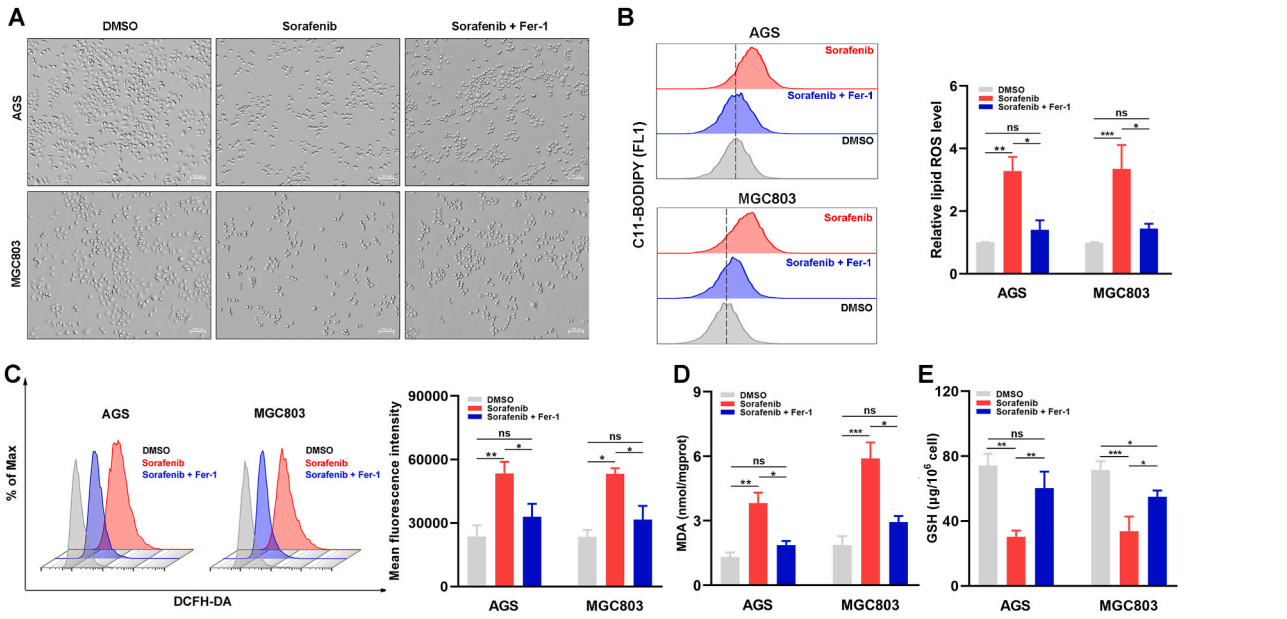

Fig. 3. Sorafenib induces ferroptosis in AGS and MGC-803 cells. **(A)** Morphologic changes of GC cells were observed under a light microscope after treatment with 10 μM sorafenib for 24 h in the absence or presence of 1 μM Fer-1. **(B-C)** Lipid peroxidation and intracellular ROS levels were detected using C11-BODIPY and DCFH-DA staining respectively, after treatment with 10 μM sorafenib for 24 h in the absence or presence of 1 μM Fer-1. **(D–E)** AGS and MGC-803 cells were incubated with 10 μM sorafenib for 24 h in the absence or presence of 1 μM Fer-1, cellular MDA and GSH levels were detected. Data are shown as the mean ± SD (n = 3). $*P < 0.05$, $**P < 0.01$, $***P < 0.001$.

3. Results

3.1. ATF2 expression is upregulated in GC and predicts an unfavorable prognosis

To investigate the expression pattern of ATF2 in GC, we first utilized the TCGA database. The results demonstrated that ATF2 mRNA expression was significantly higher in GC tissues than in normal tissues (Fig. 1A). ATF2 expression was higher in GC cell lines (SGC7901, HGC27, AGS, MGC803 and MKN45) than in a nonmalignant cell line (GES-1; Fig. 1B). In addition, we examined ATF2 protein expression in 12 pairs of fresh GC tissues and adjacent normal tissues, and found a similar result that ATF2 expression was increased in GC tissues (Fig. 1C).

Furthermore, we also evaluated ATF2 expression by IHC on a TMA containing 107 GC tissues and 22 adjacent normal tissues. Representative images with different ATF2 expression levels are shown in Fig. 1D. Notably, high ATF2 protein expression was observed in 61.7% (66/107) of GC tissues, while 63.6% (14/22) of adjacent normal tissues exhibited low ATF2 expression (Fig. 1E). To determine the clinical significance of ATF2 in GC, we analyzed the relationship between ATF2 expression and clinicopathological parameters. As shown in Table 1, the results demonstrated that increased ATF2 expression was markedly correlated with lymph node metastasis ($P = 0.003$) and distant metastasis ($P = 0.034$). In addition, overall survival (OS) analysis demonstrated that GC patients with increased ATF2 expression had a shorter survival time than those with decreased ATF2 expression (log-rank $P = 0.011$, Fig. 1F). Similarly, high ATF2 expression associated with poor outcome was also verified in a large cohort using the KM plotter database (log-rank $P = 0.005$, Fig. 1G). Subsequently, Cox regression was performed for both univariate and multivariate processes, including sex, age, tumor location, tumor size, depth of invasion, lymph node metastasis, differentiation, TNM stage, and ATF2 expression. Univariate Cox regression analysis showed that lymph node metastasis ($P = 0.005$), TNM stage ($P = 0.039$) and ATF2 expression ($P = 0.013$) were significantly correlated with the OS of GC patients (Table 2). Multivariate Cox regression analysis showed that lymph node metastasis ($P = 0.034$) and ATF2 expression ($P = 0.045$) were independent prognostic factors for the OS of GC patients (Table 2). Collectively, these results indicate that ATF2 expression is upregulated in GC and represents a valuable predictive biomarker for OS.

3.2. Knockdown of ATF2 expression suppresses GC cell malignant phenotypes

To elucidate the role of ATF2 in GC, further investigation was conducted with a series of functional assays. First, according to the expression level of ATF2 in GC cell lines, we chose the MGC803 cell line to knockdown ATF2, and the AGS cell line was selected to overexpress ATF2. The efficiency of ATF2 knockdown and overexpression was confirmed by qRT−PCR and western blot analysis (Fig. 2A and B). The results of the CCK-8 assay showed that ATF2 knockdown significantly decreased cell proliferative capacity, although ATF2 overexpression had no significant effect (Fig. 2C and D). As shown in Fig. 2E, ATF2 overexpression significantly enhanced the migration but not the invasion of GC cells. Notably, ATF2 knockdown dramatically attenuated the migration and invasion capacities of GC cells (Fig. 2F). Taken together, these results suggest that ATF2 knockdown had a much greater effect on GC cell malignant phenotypes than ATF2 overexpression in vitro.

3.3. Sorafenib induces ferroptosis and activates ATF2 expression in GC cells

Due to a previous study indicating the uncertainty in sorafenib-induced ferroptosis [12], we first investigated whether sorafenib induced ferroptosis in GC cells. As shown in Fig. 3A, after treatment with 10 μM sorafenib for 24 h, the morphology of AGS and MGC803 cells both shrank, became round and were loosely arranged. Treatment with sorafenib could sharply decrease the proliferation rate relative to untreated GC cells, while cotreatment with a ferroptosis inhibitor (Fer-1) partly reversed these changes (Fig. S1). Consistently, the live/dead cell staining of MGC803 cells revealed a similar result (Fig. S2). Treatment with sorafenib led to an increase in total cellular ROS and lipid ROS compared to the control group (Fig. 3B and C). Furthermore, incubation with sorafenib resulted in a dramatic increase in MDA but a decrease in GSH,

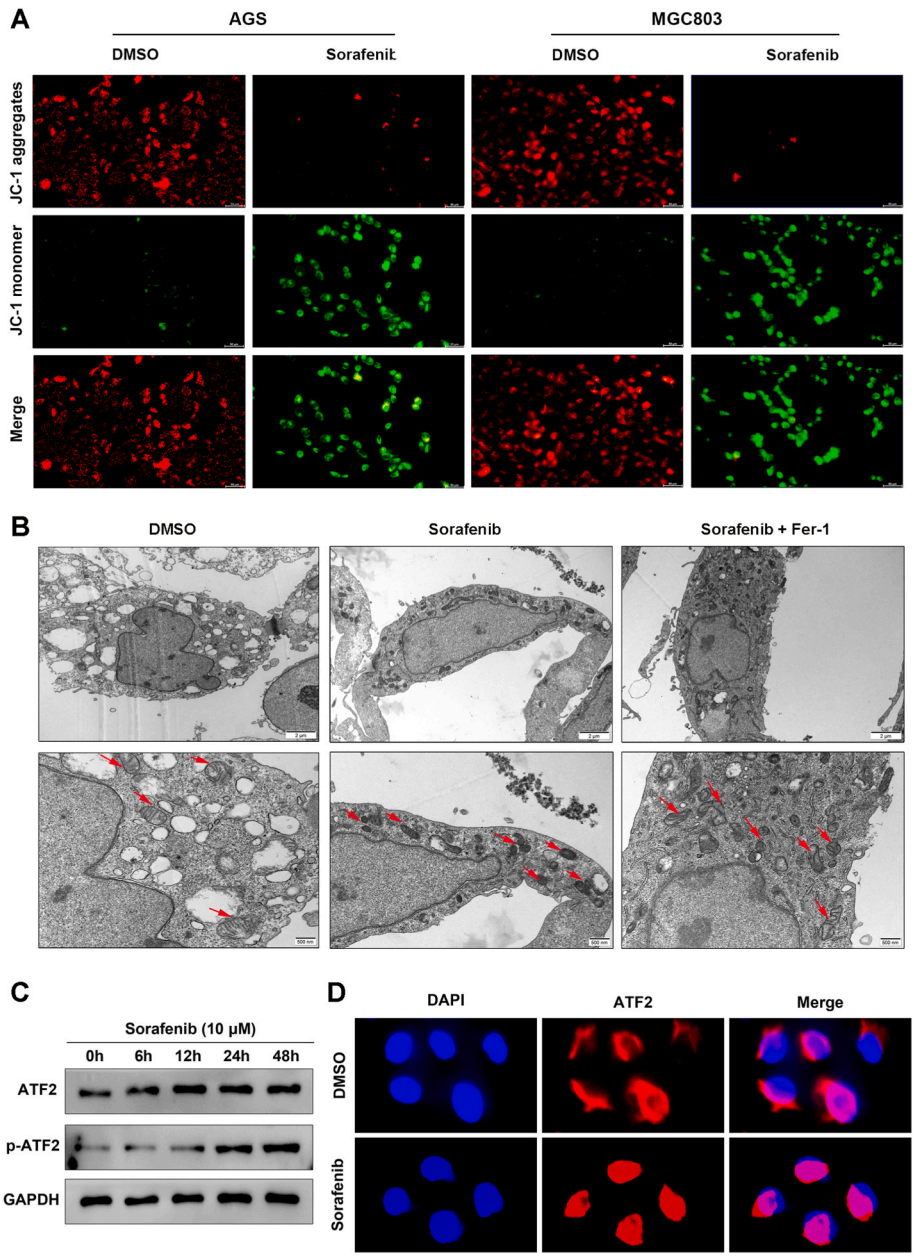

Fig. 4. Sorafenib treatment increases ATF2 expression and promotes its nuclear translocation in GC cells. **(A)** Mitochondrial membrane potential was detected with JC-1 staining after treatment with 10 μM sorafenib for 24 h. Red fluorescence (JC-1 aggregate form) represents normal membrane potential, and green fluorescence (JC-1 JC-1 monomer form) represents mitochondrial membrane potential depolarization. **(B)** The morphology of MGC803 cells was observed via TEM after treatment with 10 μM sorafenib for 24 h in the absence or presence of 1 μM Fer-1. **(C)** The levels of ATF2, p-ATF2 and SLC7A11 proteins were assessed by western blot after treatment with10 μM sorafenib at the indicated time points in MGC803 cells. **(D)** Immunofluorescence localization of ATF2 in AGS cells after treatment with or without 10 μM sorafenib for 24 h. (For interpretation of the references to color in this figure legend, the reader is referred to the Web version of this article.)

and this effect was effectively inhibited by Fer-1 (Fig. 3D and E). Given that ferroptosis is closely related to mitochondrial function, we next examined changes in mitochondrial membrane potential (MMP) and morphology. The results of JC-1 staining showed that sorafenib treatment significantly decreased the MMP compared with that in the control group (Fig. 4A). In addition, TEM revealed significantly decreased or absent mitochondrial cristae and increased mitochondrial membrane density in sorafenib-treated MGC803 cells (Fig. 4B). These results demonstrate that sorafenib can induce ferroptotic cell death in GC cells.

As a pivotal stress-response transcription factor, the change in ATF2 expression in sorafenib-induced ferroptosis remains unknown. As shown in Fig. 4C, sorafenib treatment increased ATF2 expression, especially the phosphorylated form. Notably, representative immunofluorescence showed that ATF2 was much more highly expressed in the nucleus upon stimulation with sorafenib (Fig. 4D). Therefore, sorafenib-induced ferroptosis may promote ATF2 nuclear translocation and enhance ATF2 transcriptional activity in GC cells.

3.4. *ATF2 knockdown enhances sorafenib-induced ferroptosis in GC cells*

To understand the role of ATF2 in sorafenib-induced ferroptosis, we modulated ATF2 expression levels and assessed their effects on ferroptosis. We found that ATF2 overexpression resulted in an increased IC50 value of sorafenib in AGS cells compared to vector cells, whereas ATF2 knockdown induced a decreased IC50 value of sorafenib in MGC803 cells (Fig. 5A). During sorafenib treatment, ATF2 overexpression promoted GC cell growth, whereas ATF2 knockdown inhibited it (Fig. S3). These data indicate that ATF2 expression may affect the sensitivity of GC cells to sorafenib treatment. In addition, both sorafenib treatment and ATF2 knockdown elevated total cellular ROS and lipid ROS, and ATF2 knockdown led to a further increase in AGS cells, while ATF2 overexpression restrained the increase induced by sorafenib in MGC803 cells (Fig. 5B and C). Consistently, ATF2 overexpression caused a decrease in MDA but an increase in GSH in sorafenib-treated GC cells, while ATF2 knockdown showed the opposite results (Fig. 5D and E). Finally, a more intuitive microscopic morphology was obtained by TEM. The results

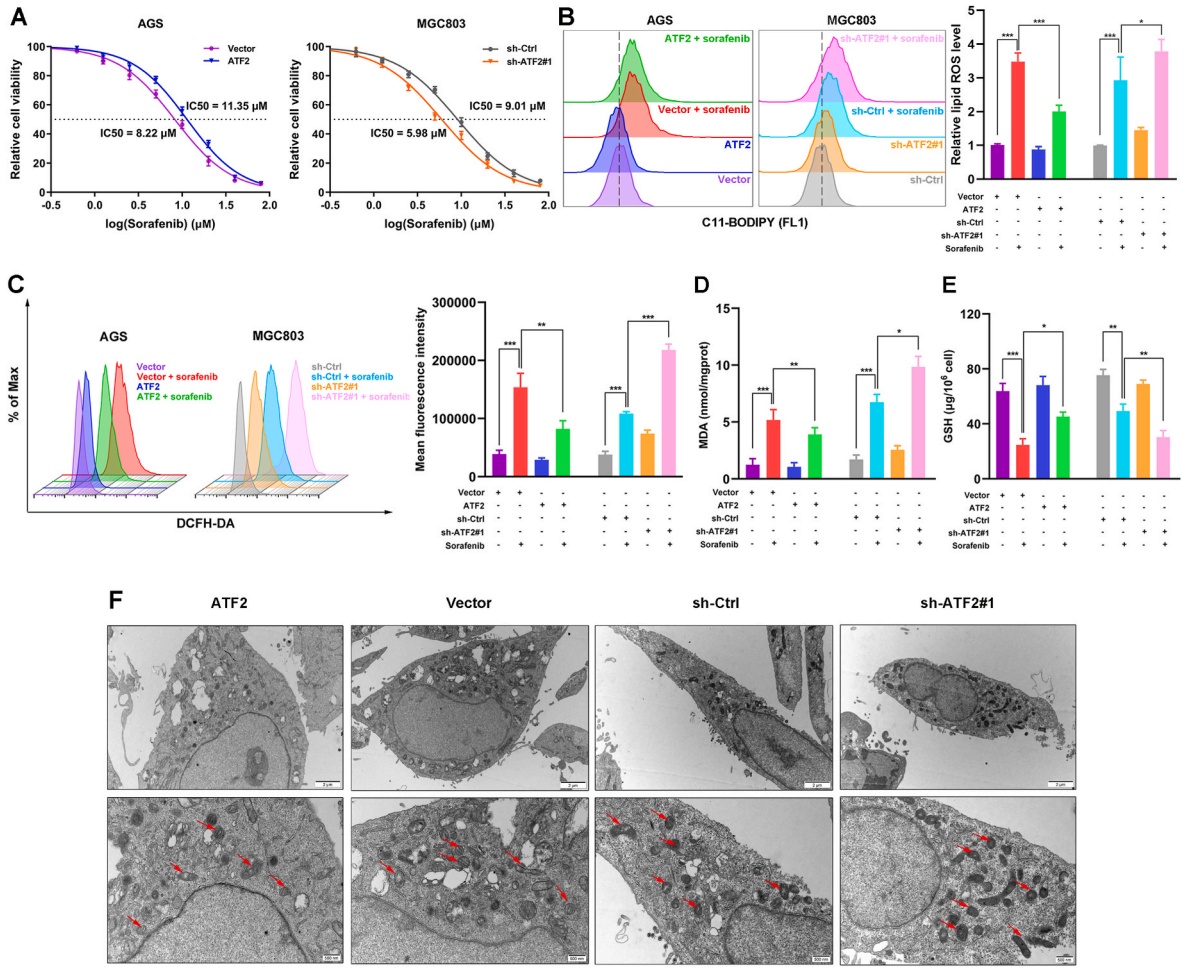

Fig. 5. ATF2 knockdown suppresses sorafenib-induced ferroptosis in GC cells. **(A)** The IC50 of GC cells after ATF2 overexpression and knockdown were determined using the CCK-8 assay. **(B-C)** Lipid peroxidation and intracellular ROS levels were detected using C11-BODIPY and DCFH-DA staining in ATF2 stably overexpression or knockdown cells with or without 10 μM sorafenib for 24 h. **(D–E)** The cellular MDA and GSH levels were assayed in ATF2 stably overexpression or knockdown cells with or without 10 μM sorafenib for 24 h. **(F)** The morphology of ATF2 stably overexpression or knockdown cells was observed via TEM after treatment with 10 μM sorafenib for 24 h. Data are shown as the mean ± SD (n = 3). $^{*}P < 0.05$, $^{**}P < 0.01$, $^{***}P < 0.001$.

showed that after sorafenib treatment, the mitochondria decreased and the membrane density was increased with vestigial cristae in ATF2 knockdown GC cells, and this effect was partly reversed by ATF2 overexpression (Fig. 5F). These findings suggest that ATF2 overexpression suppresses sorafenib-induced ferroptosis in GC cells.

3.5. ATF2 activates the transcription of HSPH1 in GC cells

To further elucidate the underlying mechanism, RNA-seq and ChIP-seq were performed to identify genome-wide DNA-binding sites and potential transcription targets for ATF2. As shown in Fig. 6A, RNA-seq analysis showed that compared with the control group, 1059 genes were upregulated and 370 genes were downregulated following ATF2 knockdown in MGC803 cells. Importantly, pathway enrichment analysis of RNA-seq data indicated that ATF2 knockdown significantly affected the ferroptosis pathway (Fig. 6B). Next, a total of 24,119 peaks corresponding to 3641 RefSeq genes were identified by ChIP-seq, of which 2.88% were located at the promoter-transcription start site (Fig. 6C). Different peak values were observed over the chromosomes, and the motifs shared between the peaks were scanned (Fig. 6D and E).

We then performed intersection analysis of RNA-seq and ChIP-seq data and screened 222 candidate transcription targets that were directly regulated by ATF2 (Fig. 7A). Among them, HSPH1 was remarkably downregulated following ATF2 knockdown (Fig. 7B). Moreover, the expression of HSPH1 in GC was significantly positively correlated with ATF2 in the TCGA dataset (Fig. 7C). As shown in Fig. 7D, the ChIP-seq data revealed significant ATF2-binding peaks in the promoter region of HSPH1 (chromosome 13 position 31,162,322–31,162,573). Thus, we hypothesized that HSPH1 may be a potential target gene of ATF2. The western blot analysis results showed that HSPH1 increased after ATF2 overexpression and decreased after ATF2 knockdown (Fig. 7E). Moreover, ChIP–qPCR further confirmed that ATF2 can bind to the promoter region of HSPH1 (Fig. 7F). These data demonstrate that ATF2 can activate HSPH1 expression by binding to its promoter.

3.6. HSPH1 interacts with and increases SLC7A11 stability in GC

Given the prominent role of heat shock proteins in ferroptosis reported by several studies [22], we sought to determine whether HSPH1 might affect SLC7A11 expression in GC. We first queried the GeneMANIA database, and the potential interactions between HSPH1 and SLC7A11 were predicted and displayed (Fig. 8A). To verify this prediction, we further performed co-IP assays and determined that HSPH1 physically interacted with SLC7A11 (Fig. 8B). Next, we adopted siRNA to knockdown HSPH1 expression (Fig. 8C) and transfected HSPH1 siRNA into AGS cells with stable ATF2 overexpression. Interestingly, we observed that HSPH1 knockdown decreased the protein expression

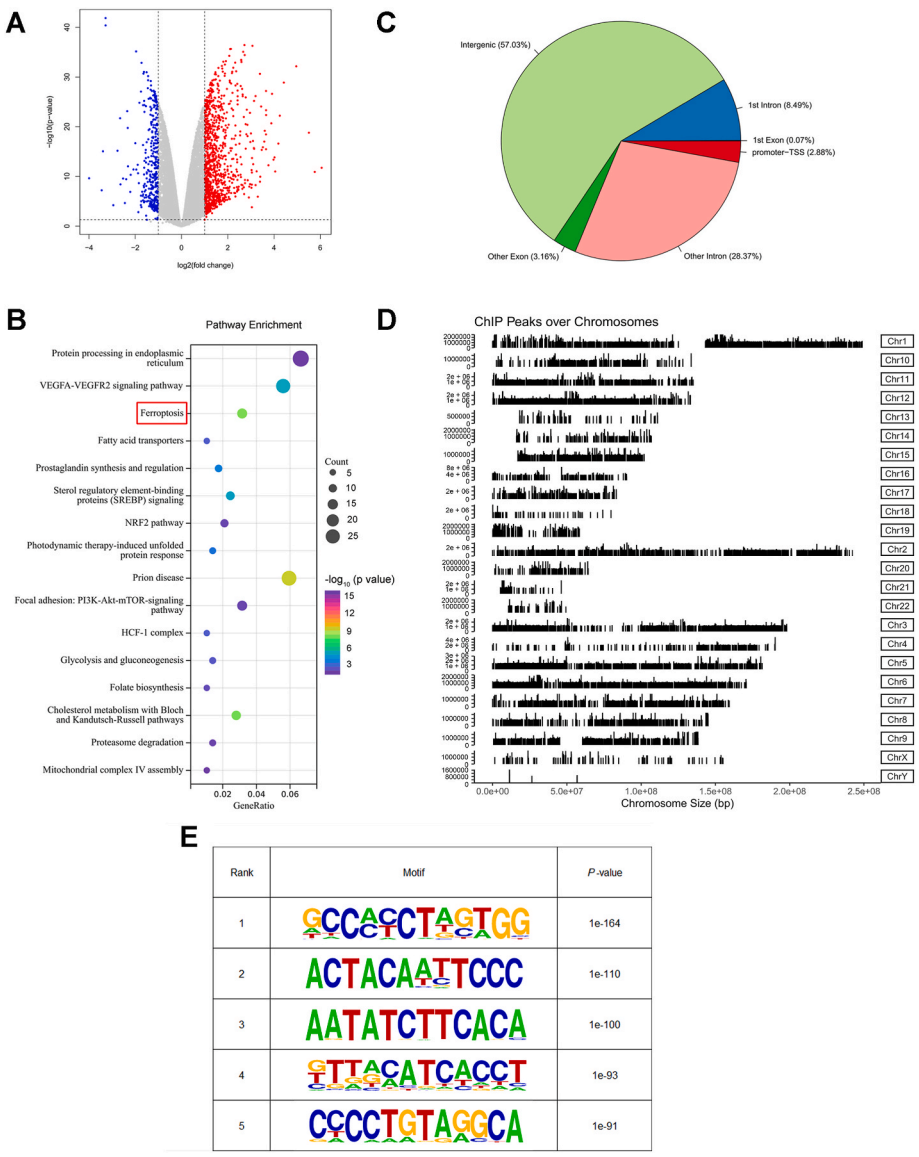

Fig. 6. Identification of genome-wide DNA binding sites and transcription targets for ATF2 by RNA-seq and ChIP-seq. **(A)** Volcano plot of differentially expressed genes in ATF2 knockdown cells compared with control cells. Red dots represent upregulated genes, and blue dots represent downregulated genes. **(B)** Pathway enrichment analysis of significantly downregulated genes. **(C)** Pie diagram shows the genomic occupancy of ATF2 binding sites as revealed by ChIP-seq in AGS cells. **(D)** The distribution of reads on chromosomes from ChIP-Seq data. **(E)** Top 5 predicted ATF2 binding motifs with the most significant *P* values. (For interpretation of the references to color in this figure legend, the reader is referred to the Web version of this article.)

levels of SLC7A11 but not the mRNA levels (Fig. 8D). Thus, we conducted a CHX chase assay to characterize the half-life of SLC7A11 protein with or without HSPH1 knockdown. Western blot analysis indicated that compared to the control group, inhibition of HSPH1 accelerated the degradation of the SLC7A11 protein in AGS cells (Fig. 8E). These results demonstrate that HSPH1 can interact with SLC7A11 and increase its expression through, at least partially, increasing SLC7A11 protein stability.

Next, we found that knockdown of HSPH1 partly abolished the effects caused by ATF2 overexpression on cellular ROS and lipid ROS (Fig. 8F and G). Consistently, co-transfection with HSPH1 siRNA significantly reversed the effects of ATF2 overexpression on cellular MDA and GSH levels in ferroptotic cell death (Fig. 8H and I). These results provide evidence that ATF2 regulates sorafenib-induced ferroptosis via HSPH1 in GC cells.

3.7. ATF2 knockdown increases the sensitivity of GC to sorafenib in vivo

Finally, to evaluate the effect of ATF2 knockdown alone and in combination with sorafenib on GC in vivo, a nude mouse xenograft model was established (Fig. 9A). Tumors formed by stable ATF2 knockdown cells were consistently smaller and lighter than those formed by control GC cells, indicating that ATF2 knockdown can effectively inhibit tumor growth in vivo (Fig. 9B). In addition, with sorafenib treatment, the volumes and weights of subcutaneous tumors were both significantly decreased (Fig. 9C and D). That is, ATF2 knockdown in combination with sorafenib treatment conferred the strongest suppression of tumor growth. To better observe potential ferroptosis, the slices of subcutaneous tumors were stained by 4-HNE, a sensitive marker of lipid peroxidation [23]. Consistently, IHC staining showed that the expression of 4-HNE in the sh-ATF2 + sorafenib group was the highest (Fig. 9E). Therefore, ATF2 knockdown enhances the anti-tumor effect of sorafenib on GC in vivo.

4. Discussion

Although the morbidity and mortality of GC have declined in recent years, the therapeutic efficacy of currently available treatment remains unsatisfactory [24]. Sorafenib-induced ferroptosis holds great potential for cancer therapy, and clarifying its underlying mechanism is urgently needed. In the present study, we found that sorafenib activated ATF2 expression and further promoted the expression of HSPH1 and decreased SLC7A11 protein degradation, thus leading to protection against lipid peroxidation (Fig. 10). Thus, targeting the ATF2/HSPH1

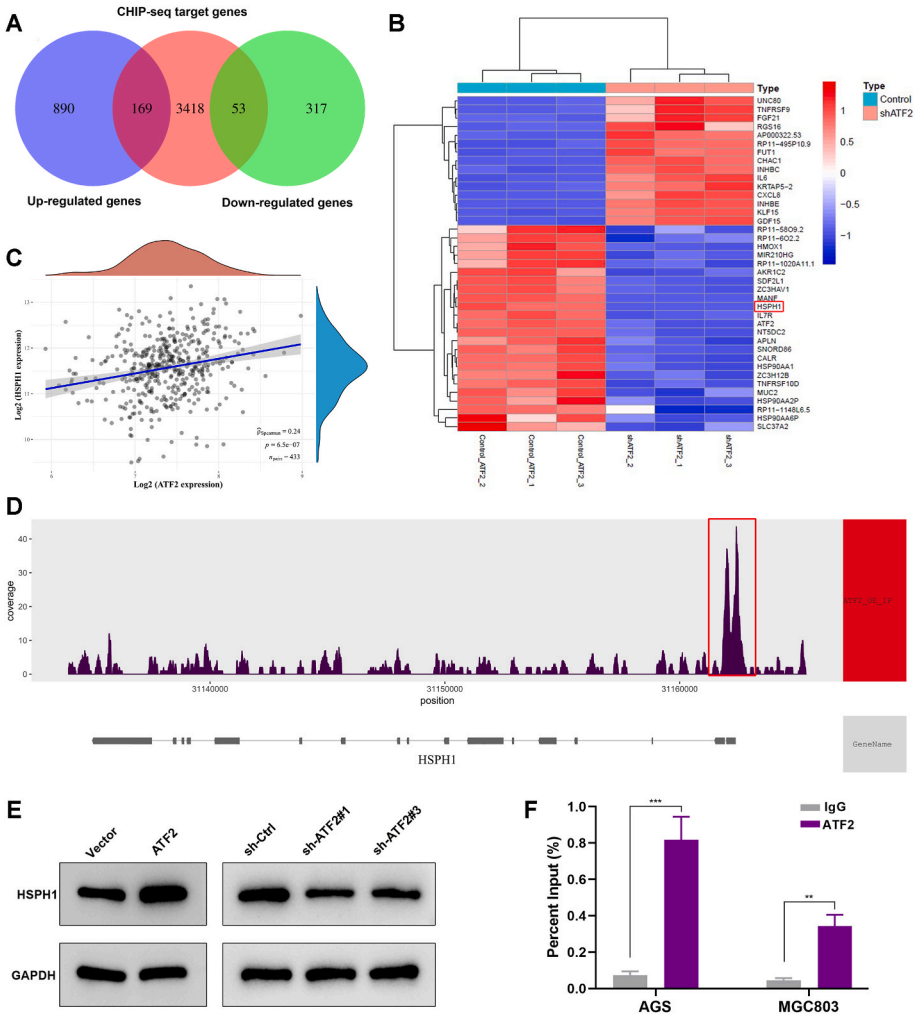

Fig. 7. ATF2 binds to the HSPH1 promoter to activate its transcription. **(A)** Venn diagram displays the genome-wide overlap analysis between RNA-seq and ChIP-seq data. **(B)** Heat map of the differentially expressed genes in ATF2 knockdown MGC803 cells compared with control cells. **(C)** The relationship between the expression of ATF2 and HSPH1 was examined by correlation analysis based on TCGA database. **(D)** ChIP-seq peaks of ATF2 enrichment at the promoter region of HSPH1. **(E)** The HSPH1 protein was analyzed by Western blot in ATF2 stably overexpression and knockdown cells. **(F)** ChIP-qPCR was used to detect the binding of ATF2 to the HSPH1 promoter in AGS and MGC803 cells. IgG was applied as a negative control. Data are shown as the mean ± SD (n = 3). $^{*}P < 0.05$, $^{**}P < 0.01$, $^{***}P < 0.001$.

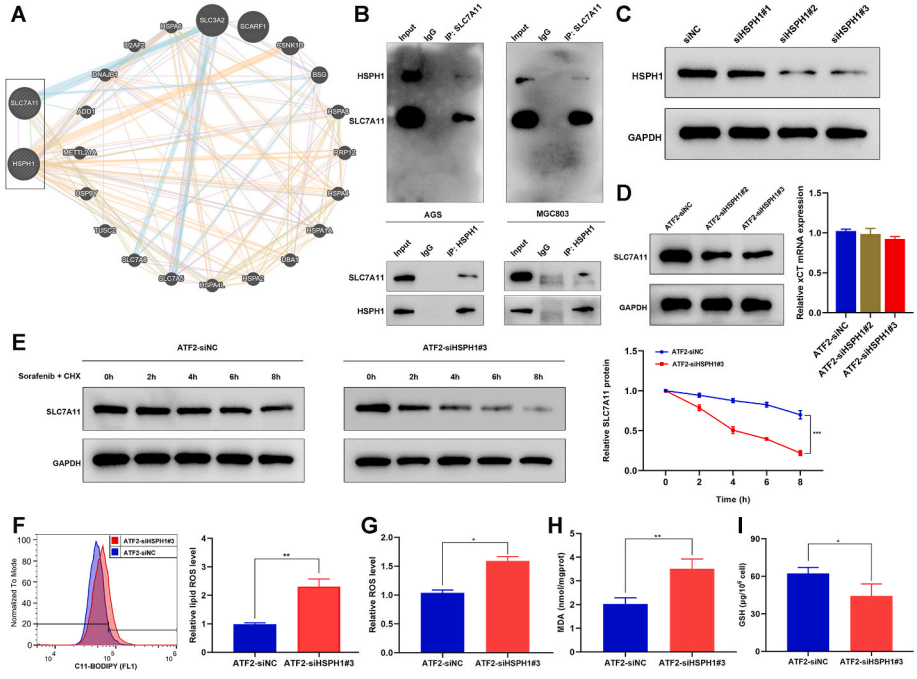

Fig. 8. HSPH1 interacts with SLC7A11 and increases its stability in GC. **(A)** The interaction between HSPH1 and SLC7A11 was displayed using GeneMANIA analysis. **(B)** Western blot analysis of the interaction between HSPH1 and SLC7A11 by co-immunoprecipitation. **(C–D)** The expression of SLC7A11 was analyzed by Western blot and qRT-PCR in ATF2 overexpression AGS cells with or without HSPH1 knockdown by siRNA transfection. **(E)** ATF2 overexpression AGS cells with or without HSPH1 knockdown were treated with 10 μM sorafenib and 20 μg/ml cycloheximide (CHX) for indicated time points, and then SLC7A11 protein level was analyzed by Western blot. **(F–G)** Lipid peroxidation and intracellular ROS levels were detected using C11-BODIPY and DCFH-DA staining after sorafenib treatment for 24 h in ATF2 overexpression AGS cells with or without HSPH1 knockdown. **(H-I)** The cellular MDA and GSH levels were assayed after sorafenib treatment for 24 h in ATF2 overexpression AGS cells with or without HSPH1 knockdown. Data are shown as the mean ± SD (n = 3). $^{*}P < 0.05$, $^{**}P < 0.01$, $^{***}P < 0.001$.

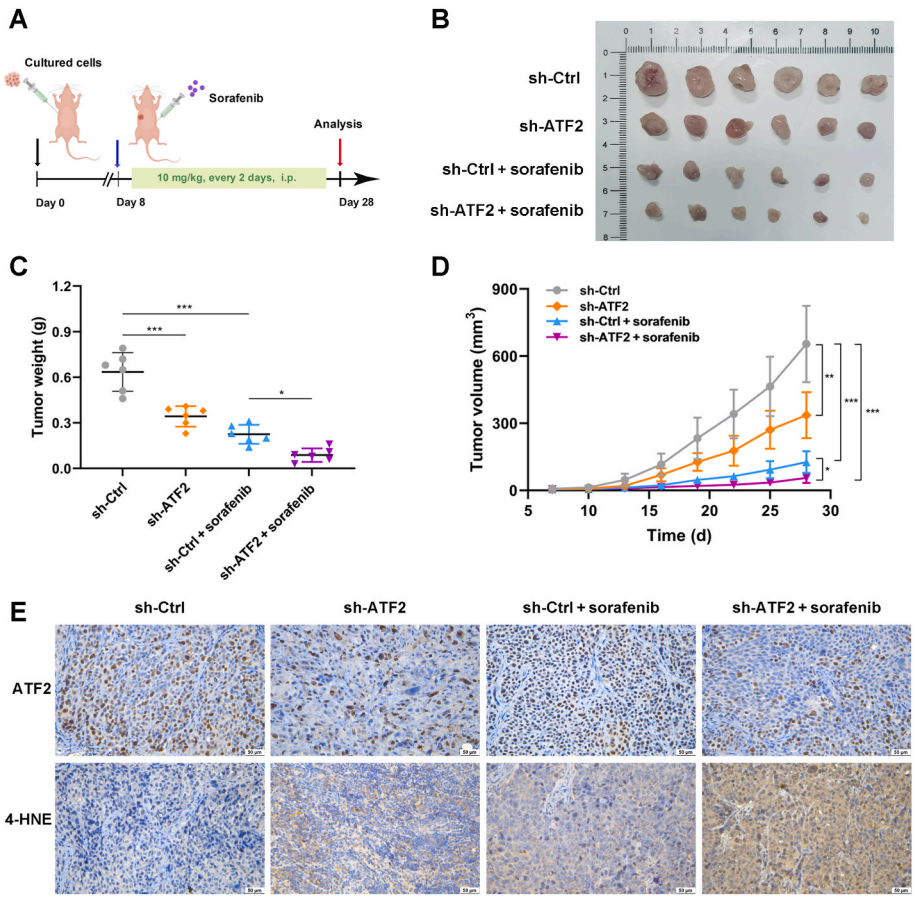

Fig. 9. ATF2 knockdown increases the sensitivity of GC to sorafenib in vivo. **(A)** Schematic description of the animal experimental design. **(B)** Representative images of dissected xenografts from the indicated groups at the end of the experiments. **(C–D)** Tumor weight of the subcutaneous xenografts and growth curves of the tumor volume in the indicated groups. **(E)** Representative immunohistochemistry images of ATF2 and 4-HNE expression in tumor tissues from the indicated groups. $^{*}P < 0.05$, $^{**}P < 0.01$, $^{***}P < 0.001$.

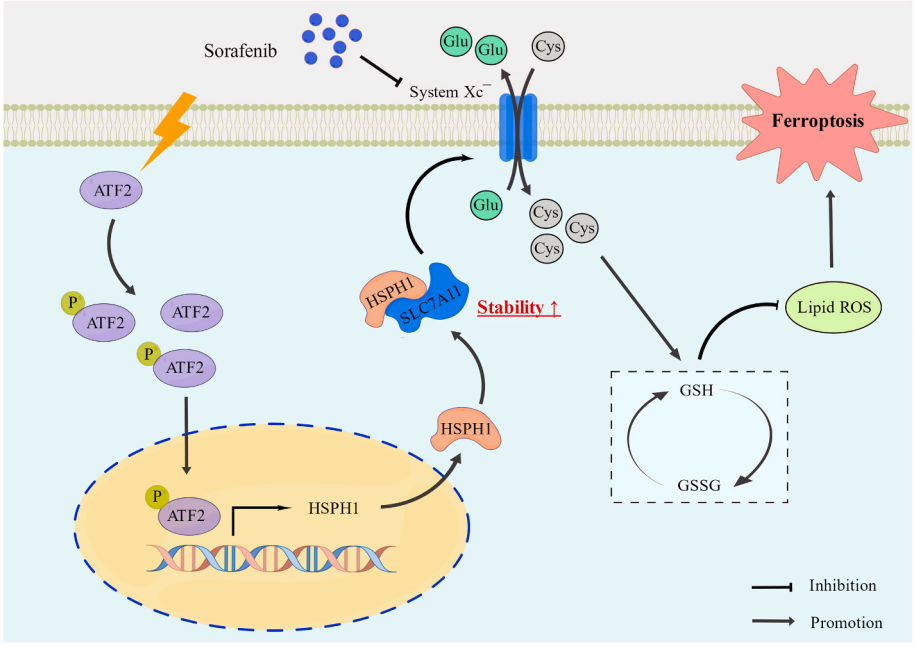

Fig. 10. Schematic diagram of the model proposed in this study. Sorafenib can induce ferroptosis and activate ATF2 expression in GC cells. Activated ATF2 translocates into the nucleus and promotes the transcription of HSPH1. Subsequently, HSPH1 binds to SLC7A11 and reduces its protein degradation, thus leading to protection against lipid peroxidation.

axis to enhance sorafenib-induced ferroptosis represents an attractive therapeutic strategy for GC.

ATF2 functions as a stress-inducible transcription factor and regulates multiple cellular processes, including the cell cycle, DNA damage response and cell death [25]. Interestingly, ATF2 can act as either a tumor suppressor in nonmetastatic skin cancer and colorectal

cancer [26,27] or as an oncogene in several tumors, such as melanoma, renal cell carcinoma and urothelial cancer [28–30]. Here, for the first time, we systematically studied the effect of ATF2 expression on malignant phenotypes, including proliferation, migration and invasion, in GC cell lines. Our data indicated that ATF2 was overexpressed in GC and that ATF2 knockdown markedly inhibited the malignant phenotype of GC cells. Additionally, high ATF2 expression was closely associated with adverse clinicopathological features and an unfavorable prognosis in patients with GC.

It has been recognized that ferroptosis can be triggered by several cancer treatments, such as chemotherapy, radiotherapy, immunotherapy and targeted therapies [31–33]. Interestingly, the unique metabolism, high active oxygen load and specific mutation of cancer cells make some of them inherently susceptible to ferroptosis [34–36]. Therefore, ferroptosis is considered a targeted vulnerability of cancer, and the use of ferroptosis inducers provides a valuable method for cancer treatment, especially in combination with traditional therapy. Previous studies have reported that sorafenib can trigger ferroptosis by inhibiting system Xc-, thereby exerting anticancer effects [7,37,38]. Conversely, another study indicated that sorafenib is not a reliable ferroptosis inducer or system Xc-inhibitor, as it failed to trigger ferroptosis across a panel of cancer cell lines [12]. In the present study, after sorafenib treatment, the changes in characteristic indicators related to ferroptosis were measured in GC cells. During this process, we noted excess ROS production and lipid peroxidation accompanied by MDA accumulation and GSH depletion. The morphological changes in mitochondria observed by TEM were consistent with the reported typical features of ferroptosis [39]. In addition, all of the above effects were partially reversed by Fer-1 treatment, indicating that sorafenib can indeed induce ferroptosis in GC cells. Notably, ATF2 was activated and translocated to the nucleus during sorafenib-induced ferroptosis. This could be explained by the response to oxidative stress that accompanies ferroptosis. In fact, except for ATF2, other cellular stress response genes, such as ATF3, ATF4 and ATF6, have also been found to be elevated during ferroptosis [40,41]. However, there are very few reports on the role of ATF2 in ferroptosis. To date, only one article has shown that ATF2 can significantly suppress bromodomain and extraterminal domain (BET) inhibitor-induced ferroptosis, thereby reducing its antitumor effect [42]. In our study, we observed that ATF2 knockdown promoted sorafenib-induced ferroptosis in GC cells by lipid peroxidation accumulation, increased ROS and MDA production and GSH depletion. Conversely, ATF2 overexpression decreased the sensitivity of GC cells to sorafenib by inhibiting ferroptosis in vitro. These findings suggest that ATF2 may play an important role in sorafenib-induced ferroptosis.

Generally, phosphorylated ATF2 translocates into the nucleus and initiates target gene transcription [43]. In this study, by combining RNA-seq and ChIP-seq data, we confirmed that HSPH1 is a direct target of ATF2. HSPH1 mainly acts as a molecular chaperone and prevents aggregation of misfolded or unfolded proteins to maintain protein homeostasis [44]. Growing evidence has suggested that HSPH1 plays a vital role in tumor progression by interacting with multiple proteins. For instance, HSPH1 can directly bind to axin to recruit protein phosphatase 2A, thereby inhibiting the hyperphosphorylation and degradation of β-catenin [45]. In addition, MyD88 protein is characteristically stabilized through an interaction with HSPH1 that leads to strong and sustained NF-κB signaling in activated B-cell diffuse large B-cell lymphoma [46]. In recent years, the roles of heat shock proteins in ferroptosis have gradually received increasing attention. One previous study demonstrated that HSPB1 overexpression suppresses erastin-mediated ferroptosis by reducing cellular iron uptake and lipid ROS production [47]. It is now clear that HSP90 regulates GPX4 degradation by inducing chaperone-mediated autophagy and plays an important role in both necroptosis and ferroptosis [48]. Likewise, HSPA5 negatively regulates ferroptosis by inhibiting GPX4 degradation, and inhibition of HSPA5 increases cell sensitivity to gemcitabine in pancreatic ductal adenocarcinoma [49]. In the current study, a potential interaction was found between HSPH1 and SLC7A11 using the GeneMANIA database. We hypothesized that HSPH1 might affect sorafenib-induced ferroptosis by regulating SLC7A11 stabilization. Our data confirmed this specific interaction between the two proteins. More importantly, HSPH1 knockdown resulted in a shortened half-life of SLC7A11 protein in GC cells. Further experiments revealed that knockdown of HSPH1 could partly abolish the effects caused by ATF2 overexpression on sorafenib-induced ferroptosis, which validated our hypothesis.

In addition, both ATF2 and HSPH1 are closely related to chemotherapy resistance in tumor cells. Loss-of-function mutation in HSPH1 confers greatly increased sensitization to oxaliplatin and 5-fluorouracil in colorectal cancer cells [50]. ATF2 was shown to repress IFNβ1 transcription and to promote resistance to chemotherapy in melanoma [51]. Importantly, previous studies have found that ATF2 knockdown can increase the sensitivity of hepatocellular carcinoma cells to sorafenib [52–54], but the underlying mechanism has remained elusive. Consistently, our data revealed that ATF2 inhibition markedly promoted sorafenib-induced ferroptosis, which in turn enhanced the anticancer effects of sorafenib on GC cells in vitro and in vivo. Thus, the current study may provide a novel perspective for overcoming sorafenib resistance.

Declaration of competing interest

The authors declare no conflict of interest.

Data availability

Data will be made available on request.

Acknowledgements

This work was supported by grants from the National Natural Science Foundation of China (NO.81874063). We would like to thank Figdraw (www.figdraw.com) for help in creating the schematic figure.

Appendix A. Supplementary data

Supplementary data to this article can be found online at https://doi.org/10.1016/j.redox.2022.102564.

References

[1] H. Sung, J. Ferlay, R.L. Siegel, M. Laversanne, I. Soerjomataram, A. Jemal, F. Bray, Global cancer statistics 2020: GLOBOCAN estimates of incidence and mortality worldwide for 36 cancers in 185 countries, CA Cancer J. Clin. 71 (2021) 209–249.
[2] F. Wang, X.L. Wei, F.H. Wang, N. Xu, L. Shen, G.H. Dai, X.L. Yuan, Y. Chen, S. J. Yang, J.H. Shi, X.C. Hu, X.Y. Lin, Q.Y. Zhang, J.F. Feng, Y. Ba, Y.P. Liu, W. Li, Y. Q. Shu, Y. Jiang, Q. Li, J.W. Wang, H. Wu, H. Feng, S. Yao, R.H. Xu, Safety, efficacy and tumor mutational burden as a biomarker of overall survival benefit in chemorefractory gastric cancer treated with toripalimab, a PD-1 antibody in phase Ib/II clinical trial NCT02915432, Ann. Oncol. 30 (2019) 1479–1486.
[3] Z. Zhang, J. Pi, D. Zou, X. Wang, J. Xu, S. Yu, T. Zhang, F. Li, X. Zhang, H. Zhao, F. Wang, D. Wang, Y. Ma, J. Yu, microRNA arm-imbalance in part from complementary targets mediated decay promotes gastric cancer progression, Nat. Commun. 10 (2019) 4397.
[4] B.R. Stockwell, J.P. Friedmann Angeli, H. Bayir, A.I. Bush, M. Conrad, S.J. Dixon, S. Fulda, S. Gascon, S.K. Hatzios, V.E. Kagan, K. Noel, X. Jiang, A. Linkermann, M. E. Murphy, M. Overholtzer, A. Oyagi, G.C. Pagnussat, J. Park, Q. Ran, C. S. Rosenfeld, K. Salnikow, D. Tang, F.M. Torti, S.V. Torti, S. Toyokuni, K. A. Woerpel, D.D. Zhang, Ferroptosis: a regulated cell death nexus linking metabolism, redox biology, and disease, Cell 171 (2017) 273–285.
[5] S.J. Dixon, Ferroptosis: bug or feature? Immunol. Rev. 277 (2017) 150–157.
[6] J. Sun, C. Zhou, Y. Zhao, X. Zhang, W. Chen, Q. Zhou, B. Hu, D. Gao, L. Raatz, Z. Wang, P.J. Nelson, Y. Jiang, N. Ren, C.J. Bruns, H. Zhou, Quiescin sulfhydryl oxidase 1 promotes sorafenib-induced ferroptosis in hepatocellular carcinoma by driving EGFR endosomal trafficking and inhibiting NRF2 activation, Redox Biol. 41 (2021), 101942.
[7] E. Lachaier, C. Louandre, C. Godin, Z. Saidak, M. Baert, M. Diouf, B. Chauffert, A. Galmiche, Sorafenib induces ferroptosis in human cancer cell lines originating from different solid tumors, Anticancer Res. 34 (2014) 6417–6422.
[8] S.J. Dixon, D.N. Patel, M. Welsch, R. Skouta, E.D. Lee, M. Hayano, A.G. Thomas, C. E. Gleason, N.P. Tatonetti, B.S. Slusher, B.R. Stockwell, Pharmacological inhibition

of cystine-glutamate exchange induces endoplasmic reticulum stress and ferroptosis, Elife 3 (2014), e02523.
[9] Y. Yamada, N. Kiyota, N. Fuse, K. Kato, H. Minami, K. Hashizume, Y. Kuroki, Y. Ito, A. Ohtsu, A phase I study of sorafenib in combination with S-1 plus cisplatin in patients with advanced gastric cancer, Gastric Cancer 17 (2014) 161–172.
[10] T. Zhao, C. Wang, X. Huo, M.L. He, J. Chen, Pterostilbene enhances sorafenib's anticancer effects on gastric adenocarcinoma, J. Cell Mol. Med. 24 (2020) 12525–12536.
[11] W. Sun, M. Powell, P.J. O'Dwyer, P. Catalano, R.H. Ansari, A.B. Benson 3rd, Phase II study of sorafenib in combination with docetaxel and cisplatin in the treatment of metastatic or advanced gastric and gastroesophageal junction adenocarcinoma: ECOG 5203, J. Clin. Oncol. 28 (2010) 2947–2951.
[12] J. Zheng, M. Sato, E. Mishima, H. Sato, B. Proneth, M. Conrad, Sorafenib fails to trigger ferroptosis across a wide range of cancer cell lines, Cell Death Dis. 12 (2021) 698.
[13] K. Kirsch, A. Zeke, O. Toke, P. Sok, A. Sethi, A. Sebo, G.S. Kumar, P. Egri, A.L. Poti, P. Gooley, W. Peti, I. Bento, A. Alexa, A. Remenyi, Co-regulation of the transcription controlling ATF2 phosphoswitch by JNK and p38, Nat. Commun. 11 (2020) 5769.
[14] E. Lau, Z.A. Ronai, ATF2 - at the crossroad of nuclear and cytosolic functions, J. Cell Sci. 125 (2012) 2815–2824.
[15] E. Lau, H. Kluger, T. Varsano, K. Lee, I. Scheffler, D.L. Rimm, T. Ideker, Z.A. Ronai, PKCepsilon promotes oncogenic functions of ATF2 in the nucleus while blocking its apoptotic function at mitochondria, Cell 148 (2012) 543–555.
[16] A. Bhoumik, P. Lopez-Bergami, Z. Ronai, ATF2 on the double - activating transcription factor and DNA damage response protein, Pigm. Cell Res. 20 (2007) 498–506.
[17] F. Liu, Z. Cheng, X. Li, Y. Li, H. Zhang, J. Li, F. Liu, H. Xu, F. Li, A novel Pak1/ATF2/miR-132 signaling Axis is involved in the hematogenous metastasis of gastric cancer cells, Mol. Ther. Nucleic Acids 8 (2017) 370–382.
[18] T. Xiaoli, W. Wenting, Z. Meixiang, Z. Chunlei, H. Chengxia, Long noncoding RNA RP11-357H14.17 plays an oncogene role in gastric cancer by activating ATF2 signaling and enhancing treg cells, BioMed Res. Int. 2021 (2021), 6635936.
[19] Q. Li, N. Liu, B. Shen, L. Zhou, Y. Wang, Y. Wang, J. Sun, Z. Fan, R.H. Liu, Helicobacter pylori enhances cyclooxygenase 2 expression via p38MAPK/ATF-2 signaling pathway in MKN45 cells, Cancer Lett. 278 (2009) 97–103.
[20] R. Sun, J. Wu, Y. Chen, M. Lu, S. Zhang, D. Lu, Y. Li, Down regulation of Thrombospondin2 predicts poor prognosis in patients with gastric cancer, Mol. Cancer 13 (2014) 225.
[21] Q. Cheng, M. Chen, M. Liu, X. Chen, L. Zhu, J. Xu, J. Xue, H. Wu, Y. Du, Semaphorin 5A suppresses ferroptosis through activation of PI3K-AKT-mTOR signaling in rheumatoid arthritis, Cell Death Dis. 13 (2022) 608.
[22] Y. Liu, L. Zhou, Y. Xu, K. Li, Y. Zhao, H. Qiao, Q. Xu, J. Zhao, Heat shock proteins and ferroptosis, Front. Cell Dev. Biol. 10 (2022), 864635.
[23] S. Dalleau, M. Baradat, F. Gueraud, L. Huc, Cell death and diseases related to oxidative stress: 4-hydroxynonenal (HNE) in the balance, Cell Death Differ. 20 (2013) 1615–1630.
[24] S.S. Joshi, B.D. Badgwell, Current treatment and recent progress in gastric cancer, CA Cancer J. Clin. 71 (2021) 264–279.
[25] P. Lopez-Bergami, E. Lau, Z. Ronai, Emerging roles of ATF2 and the dynamic AP1 network in cancer, Nat. Rev. Cancer 10 (2010) 65–76.
[26] K. Huebner, K. Erlenbach-Wuensch, J. Prochazka, I. Sheraj, C. Hampel, B. Mrazkova, T. Michalcikova, J. Tureckova, V. Iatsiuk, A. Weissmann, F. Ferrazzi, P. Kunze, E. Nalli, E. Sammer, A. Gehring, M.M. Cheema, M. Eckstein, E.M. Paap, A. Soederberg, C. Fischer, S. Paul, V. Mahadevan, B. Ndreshkjana, M.A. Meier, S. Muehlich, C.I. Geppert, S. Merkel, R. Grutzmann, A. Roehe, S. Banerjee, A. Hartmann, R. Sedlacek, R. Schneider-Stock, ATF2 loss promotes tumor invasion in colorectal cancer cells via upregulation of cancer driver TROP2, Cell. Mol. Life Sci. 79 (2022) 423.
[27] A. Bhoumik, B. Fichtman, C. Derossi, W. Breitwieser, H.M. Kluger, S. Davis, A. Subtil, P. Meltzer, S. Krajewski, N. Jones, Z. Ronai, Suppressor role of activating transcription factor 2 (ATF2) in skin cancer, Proc. Natl. Acad. Sci. U. S. A. 105 (2008) 1674–1679.
[28] S. Inoue, T. Mizushima, H. Ide, G. Jiang, T. Goto, Y. Nagata, G.J. Netto, H. Miyamoto, ATF2 promotes urothelial cancer outgrowth via cooperation with androgen receptor signaling, Endocr. Connect. 7 (2018) 1397–1408.
[29] D.S. Wu, C. Chen, Z.J. Wu, B. Liu, L. Gao, Q. Yang, W. Chen, J.M. Chen, Y. Bao, L. Qu, L.H. Wang, ATF2 predicts poor prognosis and promotes malignant phenotypes in renal cell carcinoma, J. Exp. Clin. Cancer Res. 35 (2016) 108.
[30] E. Lau, Y. Feng, G. Claps, M.N. Fukuda, A. Perlina, D. Donn, L. Jilaveanu, H. Kluger, H.H. Freeze, Z.A. Ronai, The transcription factor ATF2 promotes melanoma metastasis by suppressing protein fucosylation, Sci. Signal. 8 (2015) ra124.
[31] W. Wang, M. Green, J.E. Choi, M. Gijon, P.D. Kennedy, J.K. Johnson, P. Liao, X. Lang, I. Kryczek, A. Sell, H. Xia, J. Zhou, G. Li, J. Li, W. Li, S. Wei, L. Vatan, H. Zhang, W. Szeliga, W. Gu, R. Liu, T.S. Lawrence, C. Lamb, Y. Tanno, M. Cieslik, E. Stone, G. Georgiou, T.A. Chan, A. Chinnaiyan, W. Zou, CD8(+) T cells regulate tumour ferroptosis during cancer immunotherapy, Nature 569 (2019) 270–274.
[32] G. Lei, Y. Zhang, P. Koppula, X. Liu, J. Zhang, S.H. Lin, J.A. Ajani, Q. Xiao, Z. Liao, H. Wang, B. Gan, The role of ferroptosis in ionizing radiation-induced cell death and tumor suppression, Cell Res. 30 (2020) 146–162.
[33] G. Lei, L. Zhuang, B. Gan, Targeting ferroptosis as a vulnerability in cancer, Nat. Rev. Cancer 22 (2022) 381–396.
[34] Y. Zou, M.J. Palte, A.A. Deik, H. Li, J.K. Eaton, W. Wang, Y.Y. Tseng, R. Deasy, M. Kost-Alimova, V. Dancik, E.S. Leshchiner, V.S. Viswanathan, S. Signoretti, T. K. Choueiri, J.S. Boehm, B.K. Wagner, J.G. Doench, C.B. Clish, P.A. Clemons, S. L. Schreiber, A GPX4-dependent cancer cell state underlies the clear-cell morphology and confers sensitivity to ferroptosis, Nat. Commun. 10 (2019) 1617.
[35] V.S. Viswanathan, M.J. Ryan, H.D. Dhruv, S. Gill, O.M. Eichhoff, B. Seashore-Ludlow, S.D. Kaffenberger, J.K. Eaton, K. Shimada, A.J. Aguirre, S.R. Viswanathan, S. Chattopadhyay, P. Tamayo, W.S. Yang, M.G. Rees, S. Chen, Z.V. Boskovic, S. Javaid, C. Huang, X. Wu, Y.Y. Tseng, E.M. Roider, D. Gao, J.M. Cleary, B. M. Wolpin, J.P. Mesirov, D.A. Haber, J.A. Engelman, J.S. Boehm, J.D. Kotz, C. S. Hon, Y. Chen, W.C. Hahn, M.P. Levesque, J.G. Doench, M.E. Berens, A.F. Shamji, P.A. Clemons, B.R. Stockwell, S.L. Schreiber, Dependency of a therapy-resistant state of cancer cells on a lipid peroxidase pathway, Nature 547 (2017) 453–457.
[36] J. Wu, A.M. Minikes, M. Gao, H. Bian, Y. Li, B.R. Stockwell, Z.N. Chen, X. Jiang, Intercellular interaction dictates cancer cell ferroptosis via NF2-YAP signalling, Nature 572 (2019) 402–406.
[37] X. Sun, X. Niu, R. Chen, W. He, D. Chen, R. Kang, D. Tang, Metallothionein-1G facilitates sorafenib resistance through inhibition of ferroptosis, Hepatology 64 (2016) 488–500.
[38] Q. Wang, C. Bin, Q. Xue, Q. Gao, A. Huang, K. Wang, N. Tang, GSTZ1 sensitizes hepatocellular carcinoma cells to sorafenib-induced ferroptosis via inhibition of NRF2/GPX4 axis, Cell Death Dis. 12 (2021) 426.
[39] S.J. Dixon, K.M. Lemberg, M.R. Lamprecht, R. Skouta, E.M. Zaitsev, C.E. Gleason, D.N. Patel, A.J. Bauer, A.M. Cantley, W.S. Yang, B. Morrison 3rd, B.R. Stockwell, Ferroptosis: an iron-dependent form of nonapoptotic cell death, Cell 149 (2012) 1060–1072.
[40] L. Wang, Y. Liu, T. Du, H. Yang, L. Lei, M. Guo, H.F. Ding, J. Zhang, H. Wang, X. Chen, C. Yan, ATF3 promotes erastin-induced ferroptosis by suppressing system Xc(.), Cell Death Differ. 27 (2020) 662–675.
[41] Z. Wang, M. Li, Y. Liu, Z. Qiao, T. Bai, L. Yang, B. Liu, Dihydroartemisinin triggers ferroptosis in primary liver cancer cells by promoting and unfolded protein responseinduced upregulation of CHAC1 expression, Oncol. Rep. 46 (2021).
[42] L. Wang, Y. Chen, Y. Mi, J. Qiao, H. Jin, J. Li, Z. Lu, Q. Wang, Z. Zou, ATF2 inhibits ani-tumor effects of BET inhibitor in a negative feedback manner by attenuating ferroptosis, Biochem. Biophys. Res. Commun. 558 (2021) 216–223.
[43] K. Huebner, J. Prochazka, A.C. Monteiro, V. Mahadevan, R. Schneider-Stock, The activating transcription factor 2: an influencer of cancer progression, Mutagenesis 34 (2019) 375–389.
[44] A.S. Wentink, N.B. Nillegoda, J. Feufel, G. Ubartaite, C.P. Schneider, P. De Los Rios, J. Hennig, A. Barducci, B. Bukau, Molecular dissection of amyloid disaggregation by human HSP70, Nature 587 (2020) 483–488.
[45] N. Yu, M. Kakunda, V. Pham, J.R. Lill, P. Du, M. Wongchenko, Y. Yan, R. Firestein, X. Huang, HSP105 recruits protein phosphatase 2A to dephosphorylate beta-catenin, Mol. Cell Biol. 35 (2015) 1390–1400.
[46] C. Boudesco, E. Verhoeyen, L. Martin, C. Chassagne-Clement, L. Salmi, R. Mhaidly, C. Pangault, T. Fest, S. Ramla, F. Jardin, O.O. Wolz, A.N.R. Weber, C. Garrido, G. Jego, HSP110 sustains chronic NF-kappaB signaling in activated B-cell diffuse large B-cell lymphoma through MyD88 stabilization, Blood 132 (2018) 510–520.
[47] X. Sun, Z. Ou, M. Xie, R. Kang, Y. Fan, X. Niu, H. Wang, L. Cao, D. Tang, HSPB1 as a novel regulator of ferroptotic cancer cell death, Oncogene 34 (2015) 5617–5625.
[48] Z. Wu, Y. Geng, X. Lu, Y. Shi, G. Wu, M. Zhang, B. Shan, H. Pan, J. Yuan, Chaperone-mediated autophagy is involved in the execution of ferroptosis, Proc. Natl. Acad. Sci. U. S. A. 116 (2019) 2996–3005.
[49] S. Zhu, Q. Zhang, X. Sun, H.J. Zeh 3rd, M.T. Lotze, R. Kang, D. Tang, HSPA5 regulates ferroptotic cell death in cancer cells, Cancer Res. 77 (2017) 2064–2077.
[50] C. Dorard, A. de Thonel, A. Collura, L. Marisa, M. Svrcek, A. Lagrange, G. Jego, K. Wanherdrick, A.L. Joly, O. Buhard, J. Gobbo, V. Penard-Lacronique, H. Zouali, E. Tubacher, S. Kirzin, J. Selves, G. Milano, M.C. Etienne-Grimaldi, L. Bengrine-Lefevre, C. Louvet, C. Tournigand, J.H. Lefevre, Y. Parc, E. Tiret, J.F. Flejou, M. P. Gaub, C. Garrido, A. Duval, Expression of a mutant HSP110 sensitizes colorectal cancer cells to chemotherapy and improves disease prognosis, Nat. Med. 17 (2011) 1283–1289.
[51] E. Lau, J. Sedy, C. Sander, M.A. Shaw, Y. Feng, M. Scortegagna, G. Claps, S. Robinson, P. Cheng, R. Srivas, S. Soonthornvacharin, T. Ideker, M. Bosenberg, R. Gonzalez, W. Robinson, S.K. Chanda, C. Ware, R. Dummer, D. Hoon, J. M. Kirkwood, Z.A. Ronai, Transcriptional repression of IFNbeta1 by ATF2 confers melanoma resistance to therapy, Oncogene 34 (2015) 5739–5748.
[52] R. Rudalska, D. Dauch, T. Longerich, K. McJunkin, T. Wuestefeld, T.W. Kang, A. Hohmeyer, M. Pesic, J. Leibold, A. von Thun, P. Schirmacher, J. Zuber, K. H. Weiss, S. Powers, N.P. Malek, M. Eilers, B. Sipos, S.W. Lowe, R. Geffers, S. Laufer, L. Zender, In vivo RNAi screening identifies a mechanism of sorafenib resistance in liver cancer, Nat. Med. 20 (2014) 1138–1146.
[53] L. Luo, L. Cai, L. Luo, Z. Tang, X. Meng, Silencing activating transcription factor 2 promotes the anticancer activity of sorafenib in hepatocellular carcinoma cells, Mol. Med. Rep. 17 (2018) 8053–8060.
[54] Z. Wan, T. Liu, L. Wang, R. Wang, H. Zhang, MicroRNA-216a-3p promotes sorafenib sensitivity in hepatocellular carcinoma by downregulating MAPK14 expression, Aging (Albany NY) 12 (2020) 18192–18208.